

Low-field behavior of an XY pyrochlore antiferromagnet: emergent clock anisotropies

V. S. Maryasin,¹ M. E. Zhitomirsky,¹ and R. Moessner²

¹*Service de Physique Statistique, Magnétisme et Supraconductivité, UMR-E9001 CEA-INAC/UJF, 17 rue des Martyrs, 38054 Grenoble Cedex 9, France*

²*Max-Planck-Institut für Physik komplexer Systeme, 01187 Dresden, Germany*

(Dated: September 17, 2018)

Using $\text{Er}_2\text{Ti}_2\text{O}_7$ as a motivation, we investigate finite-field properties of an XY pyrochlore antiferromagnet. In addition to a fluctuation-induced six-fold anisotropy present in zero field, an external magnetic field induces a combination of two-, three-, and six-fold clock terms as a function of its orientation providing for a rich and controllable magnetothermodynamics. For $\text{Er}_2\text{Ti}_2\text{O}_7$, we predict a new phase transition for $\mathbf{H} \parallel [001]$, whose critical field quantifies the strength of the six-fold fluctuation contribution to the ground state energy. Unusual re-entrant transitions are also found for $\mathbf{H} \parallel [111]$. We extend these results to the whole family the XY pyrochlore antiferromagnets and show that presence and a number of low-field transitions for different orientations can be used for locating a given material in the parameter space of anisotropic pyrochlores. We use classical Monte Carlo simulations to confirm and illustrate these theoretical predictions.

PACS numbers: 75.50.Ee,

Introduction.—The Ising model is proverbially the best known model in magnetism and much of statistical mechanics [1]. It is widely used in the theory of phase transitions to describe the Z_2 symmetry breaking with applications ranging from simple ferromagnets to lattice gases and biological systems [2]. Well-known generalizations are provided by models with Z_N symmetry: Potts and clock models. Being abundantly investigated for their own sake, these models and the related symmetry breaking transitions [3] rarely appear in studies of real magnetic materials. Yet an interesting example of a Z_6 clock anisotropy was recently identified for the ordering transition in the XY pyrochlore antiferromagnet $\text{Er}_2\text{Ti}_2\text{O}_7$ [4–14]. Similar transitions may also occur in other pyrochlores $\text{Er}_2\text{Ge}_2\text{O}_7$ and $\text{Yb}_2\text{Ge}_2\text{O}_7$ with planar anisotropy [15–17].

A characteristic property of antiferromagnets with Ising anisotropy is the presence of a spin-flop transition in a magnetic field applied along the easy (Ising) axis [18]. In many cases, the spin-flop transition allows to identify the Z_2 symmetry breaking in a magnetic material on the basis of macroscopic measurements alone, without using more sophisticated microscopic techniques such as neutron or magnetic X-ray diffraction. Field-induced transitions in magnets with broken Z_N symmetry for $N > 2$ are much less documented. Therefore, understanding the interplay between the discrete Z_6 symmetry and an external field in the XY pyrochlore antiferromagnets is of significant interest from a general perspective. We find that an exquisite amount of anisotropy design is achieved by varying direction and strength of an applied field, which may induce and tune two-, three- or six-fold clock terms, producing a remarkably rich phase diagram.

$\text{Er}_2\text{Ti}_2\text{O}_7$ is the most studied member of the XY pyrochlore family. It orders below $T_c = 1.2$ K into a four-sublattice noncoplanar magnetic structure at wavevector

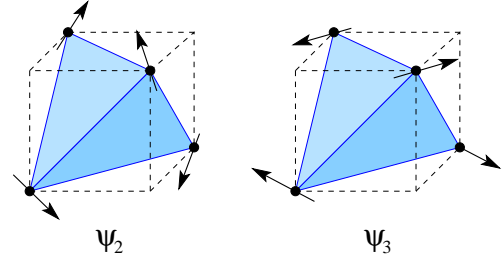


FIG. 1: (Color online) Magnetic structures in $\text{Er}_2\text{Ti}_2\text{O}_7$: the noncoplanar ψ_2 (m_1) state appearing in zero field and the coplanar ψ_3 (m_2) state stabilized by $\mathbf{H} \parallel [001]$.

$q = 0$, the so called ψ_2 state [4, 6], see Fig. 1(a). Together with the coplanar ψ_3 spin structure, Fig. 1(b), the two states transform according to the E (Γ_5) representation of the tetrahedral point group T_d . They remain degenerate at the mean-field level, producing an “accidental” emergent $U(1)$ symmetry reflected in a critical behavior in the three-dimensional XY universality class [11].

The recent surge in interest in $\text{Er}_2\text{Ti}_2\text{O}_7$ stems from the experimentally observed stabilization of the ψ_2 over the ψ_3 configuration, which appears to be an ‘order by disorder’ effect [19–22]. Thermal and quantum *fluctuations* produce an effective six-fold anisotropy in the $U(1)$ manifold spanned by the $\psi_{2,3}$ states [7–9]. The XY pyrochlore $\text{Er}_2\text{Ti}_2\text{O}_7$ appears to be a unique experimental instance of order by disorder in zero field.

Field-induced anisotropies may compete with the effect of fluctuations producing a set of extra phase transitions that are described below. Such transitions are absent in the mean-field description and their critical fields *quantify* the strength of the Z_6 anisotropy generated by fluctuations. In addition, using the information about a number of phase transitions taking place for different field orientations one can unambiguously position a given

material on the generalized phase diagram of anisotropic pyrochlores [9, 10, 23].

Model.—We use $\text{Er}_2\text{Ti}_2\text{O}_7$ as our prime example. Its low temperature magnetic properties are well described by an effective spin-1/2 Hamiltonian [7, 8]:

$$\hat{\mathcal{H}} = \sum_{\langle ij \rangle} [J_{\perp} \mathbf{S}_i^{\perp} \cdot \mathbf{S}_j^{\perp} + J_{\perp}^a (\mathbf{S}_i^{\perp} \cdot \hat{\mathbf{r}}_{ij}) (\mathbf{S}_j^{\perp} \cdot \hat{\mathbf{r}}_{ij})] - \mu_B \sum_i g_{\alpha\beta} H^{\alpha} S_i^{\beta}. \quad (1)$$

Here \mathbf{S}_i^{\perp} are spin components orthogonal to the local trigonal axis $\hat{\mathbf{z}}_i$, $\hat{\mathbf{r}}_{ij}$ denote bond directions, and $g_{\alpha\beta}$ is a staggered g -tensor with two components g_z and g_{\perp} . In accordance with the XY nature of the Er^{3+} magnetic moments, the effective Hamiltonian (1) contains only planar spin components. The omitted terms that involve S_i^z components are smaller by about an order of magnitude [7, 8]. By fitting the low- T magnetization data for $\text{Er}_2\text{Ti}_2\text{O}_7$ [24], we obtain $J_{\perp} = 0.2$ meV, $J_{\perp}^a = 0.3$ meV, $g_{\perp} = 6$, and $g_z/g_{\perp} \simeq 0.5$, see Supplemental Material for extra details [25]. These values agree within 10–15% with the previous estimates [8, 26].

We denote the overlap of a given spin configuration with two basis states of the E representation by m_1 (ψ_2) and m_2 (ψ_3). Under symmetry operations the two quantities transform as

$$m_1 \simeq (z^2 - \frac{1}{2}x^2 - \frac{1}{2}y^2), \quad m_2 \simeq \frac{\sqrt{3}}{2}(x^2 - y^2). \quad (2)$$

At mean-field level, the bilinear spin Hamiltonian (1) leaves a continuous degeneracy within the E manifold of spin states. The classical energy is the same for an arbitrary superposition $m_1 \cos \varphi + m_2 \sin \varphi$, thus featuring an ‘‘accidental’’ $U(1)$ symmetry. The complex combinations $m_{\pm} = m_1 \pm im_2 = me^{\pm i\varphi}$ transform under T_d symmetry operations as

$$\hat{C}_3^{[111]} m_{\pm} = e^{\mp 2\pi i/3} m_{\pm}, \quad \hat{\sigma}_d^{[110]} m_{\pm} = m_{\mp}. \quad (3)$$

The allowed terms in the Landau free energy correspond to invariants constructed from m_1, m_2 that must be also symmetric under time-reversal. The φ -dependent terms lift the $U(1)$ degeneracy. In zero field, the leading term appears at sixth order:

$$E_6\{\mathbf{m}\} = -\frac{a_6}{2}(m_+^6 + m_-^6) = -A_6 \cos 6\varphi, \quad (4)$$

generated by quantum and thermal fluctuations. Specifically, the quantum spin-wave correction to the ground state energy is well represented for $J_{\perp}^a/J_{\perp} \geq 0.5$ by Eq. (4) with

$$A_6 = \frac{2J_{\perp} + J_{\perp}^a}{288} \epsilon^3 S N, \quad \epsilon = \frac{J_{\perp} - \frac{1}{4}J_{\perp}^a}{J_{\perp} + \frac{1}{2}J_{\perp}^a}, \quad (5)$$

where $S = 1/2$ is an effective spin and N is the total number of sites [27]. For $J_{\perp}^a/J_{\perp} < 4$, A_6 is positive and the anisotropy selects six ψ_2 states with $\varphi_n = \pi n/3$. Note, that additional terms in the spin Hamiltonian may modify Eq. (5) but leave the expression (4) intact.

Finite-field behavior.—Applying the symmetry rules (3) one can construct energy invariants in a finite field. The lowest-order invariant is

$$E_2\{\mathbf{m}, \mathbf{H}\} = \frac{a_2}{2} [m_+^2 (e^{2\pi i/3} H_x^2 + e^{-2\pi i/3} H_y^2 + H_z^2) + \text{c.c.}]. \quad (6)$$

An external field induces a 2φ -harmonic in the angular-dependent part of the free energy. For $\mathbf{H} \parallel [001]$ and $\mathbf{H} \parallel [110]$, the expression (6) is further simplified to

$$E_2^{[001]} = A_2 H^2 \cos 2\varphi, \quad E_2^{[110]} = -\frac{1}{2} A_2 H^2 \cos 2\varphi. \quad (7)$$

The anisotropy has opposite signs for the two orientations, leading to different sequences of field-induced phases and transitions.

Direct minimization of the classical energy (1) yields

$$A_2 = \frac{(g_{\perp} \mu_B)^2 N}{8(2J_{\perp} + J_{\perp}^a)}. \quad (8)$$

Since $A_2 > 0$, the field effect appears to be rather straightforward for $\mathbf{H} \parallel [110]$: two domains of the ψ_2 state corresponding to $\varphi = 0, \pi$ are energetically selected in $\text{Er}_2\text{Ti}_2\text{O}_7$ and remain stable up to the transition into a fully polarized state at $H = H_s$. In contrast, for $\mathbf{H} \parallel [001]$, the field-induced anisotropy E_2 competes with the zero-field term (4) producing an extra transition at

$$H_c = 3\sqrt{A_6/A_2}. \quad (9)$$

Transformation of the magnetic structure can be concisely represented by a dot position on a circle showing the evolution within the $U(1)$ -manifold of E -states, see Fig. 2. Below H_c , there are four magnetic domains corresponding to $4 \cos^2 2\varphi = 1 + A_2 H^2 / (3A_6)$. The broken rotational symmetry is partially restored at $H = H_c$ and there remain only two equilibrium states with $\varphi = \pm\pi/2$. These nearly coplanar ψ_3 magnetic structures lie in the plane orthogonal to the field direction similar to the canted spin-flop state of ordinary antiferromagnets.

We use the full expression for the field-induced anisotropy to calculate H_c versus J_{\perp}^a/J_{\perp} at $T = 0$, see [25] for further details. Results shown in the top-left panel of Fig. 2 were obtained with $J_{\perp} = 0.2$ meV and $g_{\perp} = 6$. For $\text{Er}_2\text{Ti}_2\text{O}_7$, the transition into the ψ_3 state takes place in a rather weak field $H_c \approx 0.2$ T compared to $H_s = 1.7$ T. Smallness of H_c reflects the strength of the order by disorder effect and by measuring H_c it is possible to verify presence of other contributions to E_6 produced, *e.g.*, by virtual crystal-field excitations [26].

For $J_{\perp}^a/J_{\perp} > 4$, the quantum anisotropy (4) changes sign, stabilizing ψ_3 states in zero field. Accordingly, the

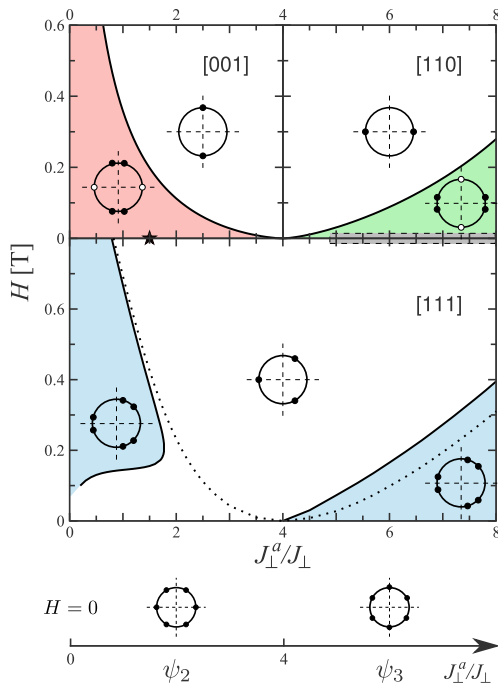


FIG. 2: Color online) Low-field transitions in the XY pyrochlore antiferromagnet at $T = 0$ as a function of J_{\perp}^a/J_{\perp} ($J_{\perp} = 0.2$ meV, $g_{\perp} = 6$). Top panels: $\mathbf{H} \parallel [001]$ and $[110]$; intermediate panel: $\mathbf{H} \parallel [111]$. Circles with full dots show the $U(1)$ manifold of $E(\Gamma_5)$ states and equilibrium values of angle φ . Light dots denote energetically unfavorable domains. A star on the J_{\perp}^a/J_{\perp} axis indicates the value appropriate for $\text{Er}_2\text{Ti}_2\text{O}_7$. The shaded area for $J_{\perp}^a/J_{\perp} > 4$ shows the parameter region proposed for $\text{Er}_2\text{Ge}_2\text{O}_7$ and $\text{Yb}_2\text{Ge}_2\text{O}_7$. The dotted line corresponds to a single transition exhibited by the classical model.

finite-field behavior is interchanged between the two field orientations: continuous evolution is expected for $\mathbf{H} \parallel [001]$, whereas an extra transition into the ψ_2 state occurs for $\mathbf{H} \parallel [110]$, see the top-right panel of Fig. 2. This range of microscopic parameters may be relevant for the other XY pyrochlores, $\text{Er}_2\text{Ge}_2\text{O}_7$ and $\text{Yb}_2\text{Ge}_2\text{O}_7$ [15–17]. Our results show that the actual identification of ψ_3 of ψ_2 magnetic structures in zero field may be obtained by measuring a low-field transition either in $\mathbf{H} \parallel [110]$ or in $\mathbf{H} \parallel [001]$ geometries.

For $\mathbf{H} \parallel [111]$, the second-order invariant (6) vanishes in accordance with the C_3 rotation symmetry about the field direction, so that selection of the phase φ is determined by higher-order terms. One such invariant describes the H^2 -correction to the six-fold anisotropy (4). Importantly, it comes with a positive sign, reducing stability of the ψ_2 states. Explicit minimization of the classical energy (1) yields

$$E_6^{[111]} = \frac{(g_{\perp}\mu_B H)^2 N}{8(2J_{\perp} + J_{\perp}^a)} \epsilon^2 \cos 6\varphi = A'_6 H^2 \cos 6\varphi. \quad (10)$$

In addition, another invariant dominates the behavior in

strong fields:

$$E_3\{\mathbf{m}, \mathbf{H}\} = \frac{a_3}{2} H_x H_y H_z (m_+^3 + m_-^3) = A_3 H^3 \cos 3\varphi. \quad (11)$$

This term selects three of six domains of the ψ_2 state in accordance with the remaining C_3 symmetry. We find numerically $A_3 > 0$, hence, the three-fold anisotropy favors $\varphi = \pm\pi/3, \pi$. Another consequence of the cubic invariant (11) is changing the nature of the high-field transition into a polarized state from second to first order accompanied by a small magnetization jump [25].

The energy of the E -states in a magnetic field $\mathbf{H} \parallel [111]$ is given by the sum of three contributions

$$E(\varphi) = (A'_6 H^2 - A_6) \cos 6\varphi + A_3 H^3 \cos 3\varphi. \quad (12)$$

The possible minima of (12) are determined by the dimensionless parameter

$$\kappa = \frac{4(A'_6 H^2 - A_6)}{A_3 H^3}. \quad (13)$$

For $\kappa < 1$ the energy minimum is reached for the three ψ_2 states with $\varphi = \pm\pi/3, \pi$. Asymmetric solutions given by $\cos 3\varphi = -1/\kappa$ appear for $\kappa > 1$. The actual field evolution of the antiferromagnetic state in an XY pyrochlore depends on the relative strength of three anisotropy parameters. For $J_{\perp}^a/J_{\perp} < 4$, the low-field ($\kappa \rightarrow -\infty$) states and the high-field states ($\kappa \approx 0$) are symmetric ψ_2 states. Therefore, we expect either no or two consecutive phase transitions. On the other hand, for $J_{\perp}^a/J_{\perp} > 4$ the low-field limit ($\kappa \rightarrow \infty$) corresponds to asymmetric solutions and upon increasing magnetic field one finds a single second-order transition.

We further analyze $E(\varphi)$ using complete expressions for A_6 and A'_6 and numerically determined A_3 [25]. The obtained phase boundaries are shown in the middle panel of Fig. 2. For $\text{Er}_2\text{Ti}_2\text{O}_7$ with $J_{\perp}^a/J_{\perp} = 1.5$ we find two phase transitions at $H_{c1} \approx 0.15$ T and $H_{c2} \approx 0.4$ T with an intermediate asymmetric phase. Remarkably, this material has a ratio of exchange constants close to the critical value $(J_{\perp}^a/J_{\perp})_c \approx 1.74$ beyond which the three ψ_2 states are stable in the whole range of fields. The critical value itself depends on the strength of the Z_6 anisotropy and additional contributions beyond quantum effects may shift $(J_{\perp}^a/J_{\perp})_c$ to smaller values. Such a scenario can be realized at finite temperatures since thermal fluctuations will further increase A_6 . Thus, observation of a double field transition in $\text{Er}_2\text{Ti}_2\text{O}_7$ may be restricted to low temperatures. In contrast, a single field transition for $J_{\perp}^a/J_{\perp} > 4$ is a robust feature and is present for all $T < T_c$.

Monte Carlo simulations.—To confirm the existence of unusual field-induced transitions in the XY pyrochlore antiferromagnet, we have performed the classical Monte Carlo (MC) simulations of the Hamiltonian (1) by replacing spins with unit vectors. This method does not allow

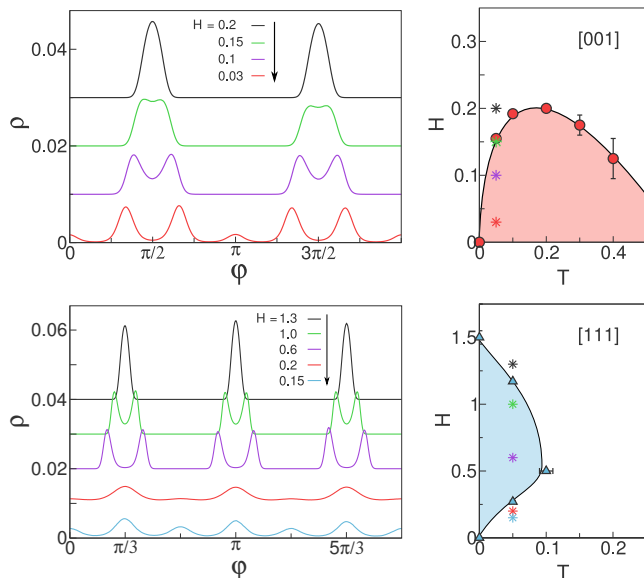


FIG. 3: (Color online) Monte Carlo results for two field orientations $\mathbf{H} \parallel [001]$ (upper row) and $\mathbf{H} \parallel [111]$ (lower row). Left plots show histograms for the angle φ collected at $T = 0.05$. Histograms for larger fields are progressively offset by $\Delta\rho = 0.01$. Right plots show phase diagrams in the relevant parts of the H - T plane. Magnetic fields chosen for histograms are indicated by stars.

to obtain the actual phase diagram of $\text{Er}_2\text{Ti}_2\text{O}_7$ since the classical model (1) lacks the Z_6 anisotropy at $T = 0$ and $H = 0$. Still, finite temperature MC results are illustrative of the generic behavior expected in real materials. In accordance with the magnetization fits, we set $J_\perp = 1$, $J_\perp^a = 1.5$, $g_\perp = 1$, and $g_z = 0.5$. Periodic clusters with $N = 4L^3$ spins up to $L = 24$ were used for simulations. The same hybrid MC algorithm was adopted as in our previous works [11, 27].

In the MC simulations we determine statistical averages of the total order parameter $m = \langle (m_1^2 + m_2^2)^{1/2} \rangle$ and the clock order parameters m_p', m_p''

$$m_p' + im_p'' = \langle (m_1 + im_2)^p \rangle / m^{p-1} = m \langle e^{ip\varphi} \rangle \quad (14)$$

with $p = 2, 3, 6$. For $\mathbf{H} \parallel [001]$, the MC results are summarized on the two upper plots in Fig. 3. We focus on the low- T /low- H part of the phase diagram ($T_c \approx 0.79$, $H_s \approx 6.45$). The transition with a loss of the mirror symmetry at $H = H_c$ is illustrated by the behavior of the probability distribution function $\rho(\varphi)$ in the E -manifold of states (left plot). At $H = 0.2$ and $T = 0.05$, $\rho(\varphi)$ has two sharp maxima corresponding to the ψ_3 states with $\varphi = \pi/2$ and $3\pi/2$. At a lower field $H = 0.15$, each of them splits into a pair of peaks, which move further apart as H is decreased. The proper order parameter for this transition is m_2'' . From the crossing of the corresponding Binder cumulants we determine $H_c = 0.156(2)$. The temperature dependence of the transition field $H_c(T)$ is shown on the upper right plot. In the classical model,

the order by disorder effect is present only at $T > 0$ and the transition field vanishes as $T \rightarrow 0$. In the opposite limit $T \rightarrow T_c$, the critical field again goes down because the six-fold anisotropy $E_6 \propto m^6$ contains a higher power of the order parameter than the field-induced $E_2 \propto m^2$.

The MC results for $\mathbf{H} \parallel [111]$ are presented in the two lower plots in Fig. 3. At $H = 1.3$, the distribution function has three peaks at $\varphi_n = \pi(2n+1)/3$ corresponding to the three high-field domains of the ψ_2 state. As the field decreases, the peaks first split and then recombine again at lower fields. Using the m_3'' order parameter, we locate the transition fields at $H_{c1} = 0.27(1)$ and $H_{c2} = 1.171(3)$ for $T = 0.05$. The relevant part of the H - T phase diagram is shown on the lower right plot. The low-symmetry phase is present only for $T \leq 0.1$. At higher temperature, the six-fold anisotropy generated by thermal fluctuations is sufficiently strong to suppress the transitions completely. The MC results for an extended range of fields and temperatures are provided in Supplemental Material [25].

Conclusions.—Using analytic and symmetry arguments supported by Monte Carlo simulations we have demonstrated that the interplay between Z_6 anisotropy and an external magnetic field leads to a series of orientation-dependent transitions in the XY pyrochlore antiferromagnet $\text{Er}_2\text{Ti}_2\text{O}_7$ and other members of this family. Presence of a low-field transition for $\mathbf{H} \parallel [001]$ but not for $\mathbf{H} \parallel [110]$ unambiguously places a pyrochlore magnet into the $J_\perp^a/J_\perp < 4$ region of the parameter space ($J_{\pm\pm} > 0$ in notations of [8]) with the ψ_2 magnetic structure in zero field. The opposite field behavior is expected for the ψ_3 ground state stabilized for $J_\perp^a/J_\perp > 4$. These conclusions can be further corroborated by checking a number of field transitions in the $\mathbf{H} \parallel [111]$ geometry (Fig. 2). The obtained results call for additional neutron experiments on the XY pyrochlores in a magnetic field. For instance, $\text{Er}_2\text{Ti}_2\text{O}_7$ was so far studied only for the “least interesting” [110] field orientation [28, 29]. Our theory generalizes the concept of the spin-flop transition to magnetic systems with the Z_6 anisotropy. Observation of such transitions is important for determining sign and strength of the six-fold clock anisotropy induced by fluctuations.

We thank E. Lhotel and S. Sosin for valuable discussions and sharing their experimental data. This work was in part supported by DFG (SFB1143).

-
- [1] E. Ising, *Z. Physik* **31**, 253 (1925).
 - [2] P. M. Chaikin and T. C. Lubensky, *Principles of condensed matter physics*, (Cambridge University Press, Cambridge, 1995).
 - [3] J. V. José, L. P. Kadanoff, S. Kirkpatrick, and D. R. Nelson, *Phys. Rev. B* **16**, 1217 (1977).
 - [4] J. D. M. Champion, M. J. Harris, P. C. W. Holdsworth,

- A. S. Wills, G. Balakrishnan, S. T. Bramwell, E. Cizmar, T. Fennell, J. S. Gardner, J. Lago, D. F. McMorrow, M. Orendac, A. Orendacova, D. McK. Paul, R. I. Smith, M. T. F. Telling, and A. Wildes, *Phys. Rev. B* **68**, 020401(R) (2003).
- [5] J. D. M. Champion and P. C. W. Holdsworth, *J. Phys.: Condens. Matter* **16**, S665 (2004).
- [6] A. Poole, A. S. Wills, and E. Lelièvre-Berna, *J. Phys.: Condens. Matter* **19**, 452201 (2007).
- [7] M. E. Zhitomirsky, M. V. Gvozdkova, P. C. W. Holdsworth, and R. Moessner, *Phys. Rev. Lett.* **109**, 077204 (2012).
- [8] L. Savary, K. A. Ross, B. D. Gaulin, J. P. C. Ruff, and L. Balents, *Phys. Rev. Lett.* **109**, 167201 (2012).
- [9] A. W. C. Wong, Z. Hao, and M. J. P. Gingras, *Phys. Rev. B* **88**, 144402 (2013).
- [10] H. Yan, O. Benton, L. Jaubert, and N. Shannon, [arXiv:1311.3501](https://arxiv.org/abs/1311.3501).
- [11] M. E. Zhitomirsky, P. C. W. Holdsworth, and R. Moessner, *Phys. Rev. B* **89**, 140403(R) (2014).
- [12] K. A. Ross, Y. Qiu, J. R. D. Copley, H. A. Dabkowska, and B. D. Gaulin, *Phys. Rev. Lett.* **112**, 057201 (2014).
- [13] P. A. McClarty, P. Stasiak, and M. J. P. Gingras, *Phys. Rev. B* **89**, 024425 (2014).
- [14] B. Javanparast, A. G. R. Day, Z. Hao, and M. J. P. Gingras, *Phys. Rev. B* **91**, 174424 (2015).
- [15] Z. L. Dun, M. Lee, E. S. Choi, A. M. Hallas, C. R. Wiebe, J. S. Gardner, E. Arrighi, R. S. Freitas, A. M. Arevalo-Lopez, J. P. Attfield, H. H. D. Zhou and J. G. Cheng, *Phys. Rev. B* **89**, 064401 (2014).
- [16] X. Li, W. M. Li, K. Matsubayashi, Y. Sato, C. Q. Jin, Y. Uwatoko, T. Kawae, A. M. Hallas, C. R. Wiebe, A. M. Arevalo-Lopez, J. P. Attfield, J. S. Gardner, R. S. Freitas, H. D. Zhou, and J.-G. Cheng, *Phys. Rev. B* **89**, 064409 (2014).
- [17] Z. L. Dun, X. Li, R. S. Freitas, E. Arrighi, C. R. Dela Cruz, M. Lee, E. S. Choi, H. B. Cao, H. J. Silverstein, C. R. Wiebe, J. G. Cheng, and H. D. Zhou, [arXiv:1508.04489](https://arxiv.org/abs/1508.04489).
- [18] N. Majlis, *The quantum theory of magnetism*, (World Scientific, Singapore, 2007).
- [19] J. Villain, R. Bidaux, J. P. Carton and R. Conte, *J. Physique* **41**, 1263 (1980).
- [20] E. F. Shender, *Zh. Eksp. Teor. Fiz.* **83**, 326 (1982) [*Sov. Phys. JETP* **56**, 178 (1982)].
- [21] C. L. Henley, *Phys. Rev. Lett.* **62**, 2056 (1989).
- [22] R. Moessner, *Can. J. Phys.* **79**, 1283 (2001).
- [23] L. Savary and L. Balents, *Phys. Rev. Lett.* **108**, 037202 (2012).
- [24] P. Bonville, S. Petit, I. Mirebeau, J. Robert, E. Lhotel, and C. Paulsen, *J. Phys.: Condens. Matter* **25**, 275601 (2013).
- [25] see Supplemental Material.
- [26] S. Petit, J. Robert, S. Guitteny, P. Bonville, C. Decorse, J. Ollivier, H. Mutka, M. J. P. Gingras, and I. Mirebeau, *Phys. Rev. B* **90**, 060410(R) (2014).
- [27] V. S. Maryasin and M. E. Zhitomirsky, *Phys. Rev. B* **90**, 094412 (2014).
- [28] J. P. C. Ruff, J. P. Clancy, A. Bourque, M. A. White, M. Ramazanoglu, J. S. Gardner, Y. Qiu, J. R. D. Copley, M. B. Johnson, H. A. Dabkowska, and B. D. Gaulin, *Phys. Rev. Lett.* **101**, 147205 (2008).
- [29] H. B. Cao, I. Mirebeau, A. Gukasov, P. Bonville, and C. Decorse, *Phys. Rev. B* **82**, 104431 (2010).